ELEC639B Term Project: An Image Compression System with Interpolating Filter Banks

Yi Chen

Abstract

In this project, two families of filter banks are constructed, then their performance is compared with an image compression system. The one-dimensional and quincunx families of interpolating filter banks are constructed on the lifting scheme, such that they have the properties of perfect reconstruction and arbitrary numbers of vanishing moments. Then the filter banks are applied to images, and the transformed data are processed in some quantization strategies such that the performance is compared in terms of PSNR.

I. INTRODUCTION

Wavelet transforms and perfect reconstruction filter banks (PRFBs) are widely used in numerous signal processing applications including image compression, and there are various construction techniques for PRFBs [1]. The introduction of the lifting scheme by Sweldens [2] [3] provides a new way of wavelet constructions. It was motivated to build time-varying filter banks, and it also offers several advantages to the earlier approaches in the time-invariant setting [4]. Lifting also leads to fast and inplace implementation of PRFBs, and can be used in reversible integer to integer wavelet transforms.

[4] shows that families of wavelets with interpolating scaling functions can be built with two lifting steps: a predict step and an update step. The resulting filter banks have the perfect reconstruction and arbitrary numbers of dual and primal vanishing moments, if the predict and update filters satisfy certain conditions related to Neville filters.

In this project, two families of interpolating filters are built: the traditional one dimensional two channel filter banks, and the two dimensional nonseparable quincunx filter banks. Then the performance of those filters are compared within an image compression system.

This report is organized as follows. Section II provides the notation and some preliminaries, such as Neville filters and the lifting scheme. Section III states the problem studied in this project. Section IV describe how to construct the interpolating filter banks and implement the image compression system, and gives some examples. The results of the performance comparison between different wavelet transforms are given in Section V, and the conclusion is made in Section VI.

II. Notation and Background Materials

A. Notation

The notation used in this report is the same as in [4]:

1) Signal: A signal x is a sequence of real-valued numbers indexed by the index set $\mathcal{K}$

$$x = \{x_k \in \boldsymbol{R} \mid k \in \mathcal{K}\} \in \boldsymbol{R}^{\mathcal{K}}.$$

In this project, the index set $\mathcal{K} \in \boldsymbol{Z}^d$ and the signal is defined on a lattice in d-dimensional Euclidean space.

2) Linear operator and its adjoint: A linear operator is $A : l^2(\mathcal{K}) \to l^2(\mathcal{K})$, and the adjoint of A is the linear operator A^* such that $\langle Ax, y\rangle = \langle x, A^* y\rangle$ for all sequences $x, y \in l^2(\mathcal{K})$, where $\langle \cdot, \cdot \rangle$ is the standard inner product. A filter is a time invariant linear operator with the impulse response $\{a_k \mid k \in \mathcal{K}\}$.

3) Polynomial and the space: $\pi(x)$ is a multivariate polynomial with $x \in \boldsymbol{R}^d$. π is the sequence formed by evaluating $\pi(x)$ on the lattice $\boldsymbol{Z}^d$.

$$\pi = \pi\left(\boldsymbol{Z}^d\right) = \left\{\pi(k) \in k \in \boldsymbol{Z}^d\right\}$$

Π_n denotes the space of all polynomial sequences of total degree less than n.

4) Multidimensional filters: A multidimensional filter is a linear operator, where the index set $\mathcal{K} = \boldsymbol{Z}^d$. An index $k \in \boldsymbol{Z}^d$ is a vector $(k_1, \ldots, k_d)$ where $k_j \in \boldsymbol{Z}$. z is also a vector $(z_1, \ldots, z_d)$. If $\alpha = (\alpha_1, \ldots, \alpha_d)$, then

$$z^\alpha = \prod_{i=1}^{d} z_i^{\alpha_i}$$

and the size of a multi-index is

$$|n| = \sum_{i=1}^{d} n_i$$

5) Sublattices: D is a $d \times d$ matrix with integer coefficients, then $D\boldsymbol{Z}^d$ is a sublattice of $\boldsymbol{Z}^d$. There are $\det D - 1$ cosets of the form $D\boldsymbol{Z}^d + t_j$, where $t_j \in \boldsymbol{Z}^d$ and $1 \leq j \leq \det D$. These cosets satisfies

$$\boldsymbol{Z}^d = \bigcup_{j=0}^{M-1} \left(D\boldsymbol{Z}^d + t_j \right)$$

$\downarrow D : \boldsymbol{A}^{\mathcal{K}} \to \boldsymbol{A}^{D\mathcal{K}}$ is the downsmapling operator with the dilation matrix D, and its adjoint is the upsampling operator $\uparrow D$. In z-domain, the upsampling is defined as:

$$z^D = \{z^{d_1}, z^{d_2}, \ldots, z^{d_d}\}$$

where d_i is the ith column vector of the dilation matrix D.

B. Interpolating Filters

A filter H is interpolating if its impulse response satisfies $h_{D_k} = \delta_k$, which means that the impulse response is zero in all sampling points except the origin. Its z-transform can be expressed as:

$$H(z) = 1 + \sum_{i=1}^{M-1} z^{t_i} P_i \left(z^D \right)$$

When an interpolating filter is applied to an upsampled signal, the values of the original sample points remain the same and the values of the new points are the linear combination of the old ones.

A scaling function $\phi(x) \in \L_2(\boldsymbol{R}^d)$ satisfies a refinement relation:

$$\phi(x) = \sum_{k \in \mathcal{K}} h_k \phi(Dx - k)$$

where $\{h_k\}$ is the impulse response of a filter H. The scaling function is interpolating if it satisfies $\phi(k) = \delta_k$, which means it is zero in all points in the lattice except the origin. If a scaling function is interpolating, the refinement filter H is also interpolating.

C. Neville Filters

A filter P is a Neville filter of order N with shift $\tau \in \boldsymbol{R}^d$ if

$$P\pi \left(\boldsymbol{Z}^d \right) = \pi \left(\boldsymbol{Z}^d + \tau \right), \quad \text{for } \pi \in \Pi_N$$

which means if P is applied to a polynomial, it results in the same polynomial on the original lattice offset by τ.

A Neville filter P has the property that its impulse response $\{p_k\}$ satisfies

$$\sum_k p_{-k} k^n = \tau^n, \quad \text{for } |n| < N. \tag{1}$$

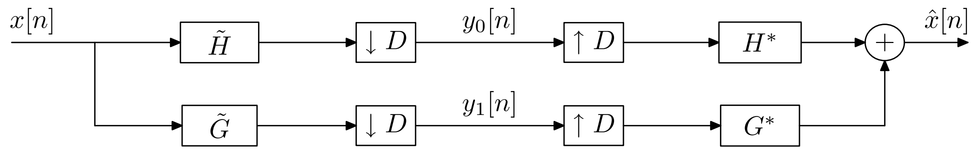

Fig. 1. A typical 2-channel UMD filter bank

This equation provides a way to calculate the coefficients of the Neville filters.

Some other important properties of the Neville filters are:

(1) If P is a Neville filter of order N with shift τ, then the adjoint P^* is a Neville filter of order N with shift $-\tau$.

(2) If P is a Neville filter of order N with shift τ, and $P^{'}$ is a Neville filter of order $N^{'}$ with shift $\tau^{'}$, then $PP^{'}$ is a Neville filter of order $\min N, N^{'}$ with shift $\tau + \tau^{'}$.

(3) If P is a Neville filter of order N with shift τ, then $Q(z) = P\left(z^D\right)$ is a Neville filter of order N with shift $D\tau$.

D. Lifting

Lifting is a way to calculate and design filter banks [2] [3]. It features reversible and inplace computation, and leads to fast implementation of the discrete wavelet transform. A UMD filter bank shown in Fig. 1 can be implemented by the lifting scheme by decomposing the polyphase matrices into a sequence of elementary matrices; each matrix represents a simple operation of the subband signals. The resulting lifting structure is illustrated in Fig. 2. Fig. 2(a) shows the analysis side of the filter bank, which consists of a set of lifting steps: prediction steps P_i and update steps U_i, and Fig. 2(b) shows the analysis side of the filter bank, which consists of a set of inverse steps.

The lifting structure is also used in building new subband decompositions from the existing ones. The basic idea behind lifting is that the new and old filter banks have the same lowpass or highpass filters. The construction begins from a trivial filter bank, and then the properties of the filter bank is enhanced using lifting steps P_i and U_i. The trivial filter bank is the polyphase transform, also referred to as the Lazy wavelet transform [2], which splits the input signal into even- and odd-indexed components. The analysis polyphase matrix $\boldsymbol{P}_a$ is then given by the product of the elementary matrices which correspond to the lifting steps:

$$\boldsymbol{P}_a = \begin{bmatrix} \tilde{H}_e & \tilde{H}_o \\ \tilde{G}_e & \tilde{G}_o \end{bmatrix} = \cdots \begin{bmatrix} 1 & U_1 \\ 0 & 1 \end{bmatrix} \begin{bmatrix} 1 & 0 \\ -P_1 & 1 \end{bmatrix}$$

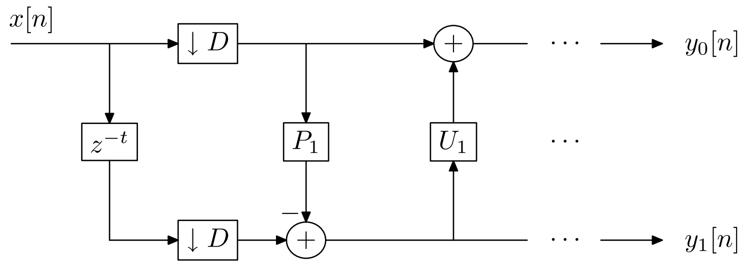

(a) Analysis side

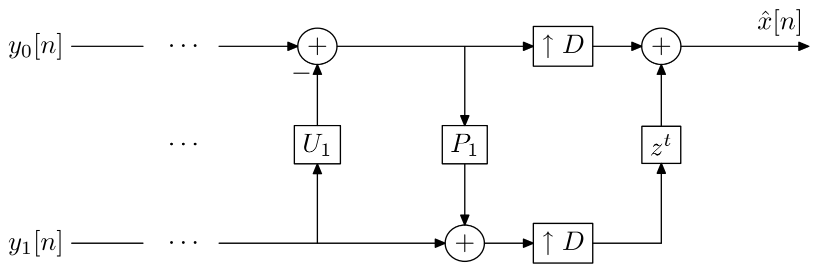

(b) Synthesis side

Fig. 2. The lifting structure of two channel filter banks

and the analysis filters are given by:

$$\tilde{H}(z) = \tilde{H}_e\left(z^D\right) + z^{-t}\tilde{H}_o\left(z^D\right)$$

$$\tilde{G}(z) = \tilde{G}_e\left(z^D\right) + z^{-t}\tilde{G}_o\left(z^D\right)$$

E. Quincunx Filters Banks

A quincunx lattice is a two dimensional nonseparable lattice with dilation matrix:

$$D = \begin{bmatrix} 1 & 1 \\ 1 & -1 \end{bmatrix}$$

Fig. 3 shows the lattices before and after the downsampler $\downarrow D$. There are other dilation matrices that result in the same sublattices, such as $\begin{bmatrix} 0 & 2 \\ 1 & 1 \end{bmatrix}$. D is better than the other dilation matrices in that $D^2 = 2\boldsymbol{I}$, which means that two levels of downsampling by D is separable.

The quincunx filter banks have the advantage that it leads to a two-channel multiresolution analysis, and the expressions of z-domain downsampling and upsampling are in a similar form to that of one dimensional filter banks. The relationship is shown in Table I. Another advantage is that they can better extract the spectrum information of images and adopts to human visual system, as they are more sensitive along the diagonal directions than the traditional separable filter banks.

TABLE I

THE RELATIONSHIP BETWEEN ONE-DIMENSIONAL AND QUINCUNX FILTER BANKS IN DOWNSAMPLING AND UPSAMPLING

	Downsampling
1-D	$Y(z) = \frac{1}{2}\left[X(z^{1/2}) + X(-z^{1/2})\right]$
Quincunx	$Y(z_1, z_2) = \frac{1}{2}\left[X \quad z_1^{1/2} z_2^{1/2}, z_1^{1/2} z_2^{-1/2} \quad + X \quad -z_1^{1/2} z_2^{1/2}, -z_1^{1/2} z_2^{-1/2} \quad \right]$
	Upsampling
1-D	$Y(z) = X(z^2)$
Quincunx	$Y(z_1, z_2) = X \quad z_1 z_2, z_1 z_2^{-1}$
	Upsampling after downsampling
1-D	$Y(z) = \frac{1}{2}\left[X(z) + X(-z)\right]$
Quincunx	$Y(z_1, z_2) = \frac{1}{2}\left[X(z_1, z_2) + X(-z_1, -z_2)\right]$

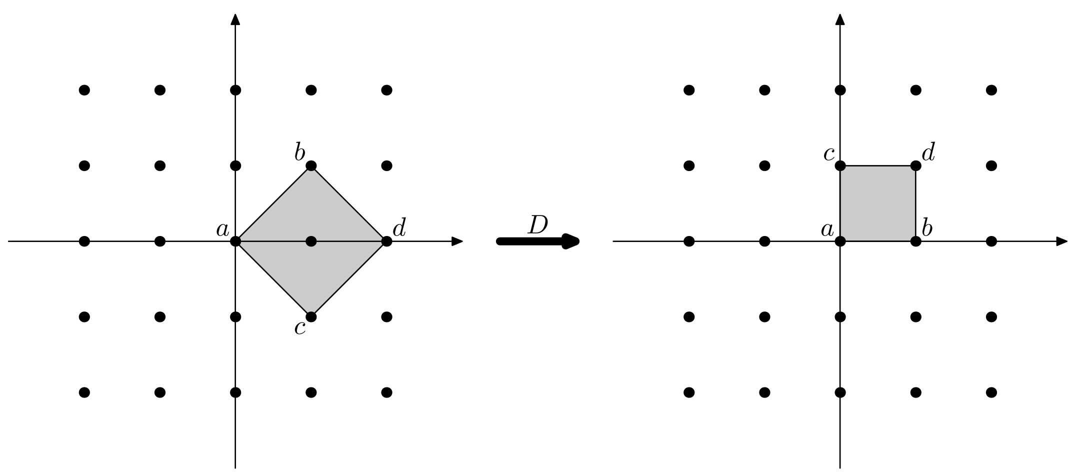

Fig. 3. Quincunx lattices before and after downsampled by D with unit cell

III. PROBLEM STATEMENT

This project includes three parts:

- Construction of interpolating filter banks
- Implementation of the compression system
- Performance comparison

The purpose of the first part, construction of interpolating filter banks, is to build two channel filter banks with analysis filters $\tilde{H}$, $\tilde{G}$, and synthesis filters H, G that satisfy three properties: perfect reconstruction, N primal vanishing moments and $\tilde{N}$ dual vanishing moments, as shown in Fig. 1. Two

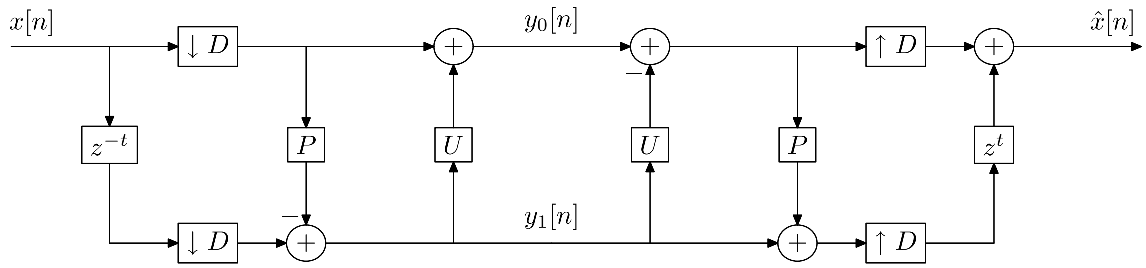

Fig. 4. 2-step lifting scheme

families of interpolating filters are built based on the lifting scheme: the traditional one dimensional and nonseparable quincunx interpolating filter bank families.

In the second part, implementation of the compression system, the wavelets constructed in the first part are applied to images, then the transformed wavelet coefficients are compressed using an encoder similar to the one in JPEG 2000 standard. In the inverse process, the compressed data is decoded and the inverse wavelet transform is implemented to reconstruct the images. At the time of writing this report, the encoder still does not work. Therefore, other methods are used to approximate a lossy coder by simply quantizing the wavelet coefficients.

The last part of this project is to compare the performance of different wavelets by computing the PSNR of the images reconstructed from quantized wavelet coefficients.

IV. METHODS

A. Construction of Filter Banks

The interpolating filter banks are constructed based on the two-step lifting scheme shown in Fig. 4. P is the predict filter and U is the update filter. These two lifting steps in the analysis side, and the corresponding inverse steps in the synthesis side are sufficient to satisfy the three properties: perfect reconstruction, dual and primal vanishing moments, and these properties can be satisfied separately [4].

- Perfect reconstruction

  This property requires that the reconstructed signal $\hat{x}[n]$ is a shifted version of the input signal $x[n]$. It is automatically satisfied for every filter bank built with lifting.

- Dual vanishing moments:

  The dual wavelets have $\tilde{N}$ vanishing moments,

$$\int t^k \tilde{\psi}(t) dt = 0, \quad \text{for } |k| < \tilde{N}$$

which means the primal scaling function can accurately approximate smooth polynomials up to order $\tilde{N}$, and the wavelet coefficients of a smooth function decays rapidly. Using the notation in Section II, it can be expressed as

$$(\downarrow)\tilde{G}\,\pi = 0 \quad \text{for} \quad \pi \in \Pi_{\tilde{N}}$$

This property is satisfied if the predict filter P is a Neville filter of order $\tilde{N}$ and shift $\tau = D^{-1}t$.

- Primal vanishing moments:

  The primal wavelets have N vanishing moments,

$$\int t^k \psi(t) dt = 0, \quad \text{for } |k| < N$$

  Using the notation in Section II, it can be expressed as

$$(\downarrow)G\,\pi = 0 \quad \text{for} \quad \pi \in \Pi_N$$

  This property is satisfied if $2U$ is a Neville filter of order N and shift $-\tau = -D^{-1}t$.

Therefore, the predict and update filters can be computed by solving the linear systems in (1). After selecting the proper predict filter P and update filter U, the analysis and synthesis polyphase matrix of the filter bank P_a and P_s can be computed as:

$$\boldsymbol{P_a} = \begin{bmatrix} \tilde{H}_e & \tilde{H}_o \\ \tilde{G}_e & \tilde{G}_o \end{bmatrix} = \begin{bmatrix} 1 - UP & U \\ -P & 1 \end{bmatrix}$$

$$\boldsymbol{P_s} = \begin{bmatrix} H_e & H_o \\ G_e & G_o \end{bmatrix} = \begin{bmatrix} 1 & P^* \\ -U^* & 1 - U^* P^* \end{bmatrix}$$

and the analysis and synthesis filters are:

$$\tilde{H}(z) = \tilde{H}_e\left(z^D\right) + z^{-t}\tilde{H}_o\left(z^D\right) = 1 - U\left(z^D\right)P\left(z^D\right) + z^{-t}U\left(z^D\right)$$

$$\tilde{G}(z) = \tilde{G}_e\left(z^D\right) + z^{-t}\tilde{G}_o\left(z^D\right) = -P\left(z^D\right) + z^{-t}$$

$$H(z) = H_e\left(z^D\right) + z^{t}H_o\left(z^D\right) = 1 + P^*\left(z^D\right)$$

$$G(z) = G_e\left(z^D\right) + z^{t}G_o\left(z^D\right) = -U^*\left(z^D\right) + z^{-t}\left(1 - U^*\left(z^D\right)P^*\left(z^D\right)\right)$$

where H is interpolating.

TABLE II

SOME OF THE ONE DIMENSIONAL NEVILLE FILTERS WITH LINEAR PHASE

	Numerator										Denominator
Order	4	3	2	1	0	-1	-2	-3	-4	-5	
2					1	1					2
2				-1	9	9	-1				2^4
6			3	-25	150	150	-25	3			2^8
8		-5	49	-245	1225	1225	-245	49	-5		2^{11}
10	35	-405	2268	-8820	39690	39690	-8820	2268	-405	35	2^{16}

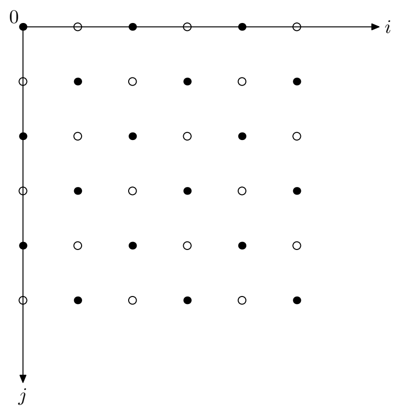

Fig. 5. Coset representative of a quincunx lattice

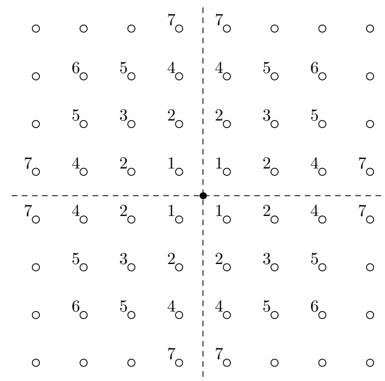

Fig. 6. The quincunx lattice in the sampled domain with neighborhoods. The point in the center represents τ that are to be interpolated

1) One Dimensional Filter Banks: In one dimensional cases, the Neville filters can be easily constructed by solving the linear systems in (1), which can be rewritten in matrix form as:

$$\begin{bmatrix} 1 & 1 & \cdots & 1 \\ k_1 & k_1+1 & \cdots & k_2 \\ \vdots & \vdots & \ddots & \vdots \\ k_1^{N-1} & (k_1+1)^{N-1} & \cdots & k_2^{N-1} \end{bmatrix} \begin{bmatrix} p_{-k_1} \\ p_{-(k_1+1)} \\ \vdots \\ p_{-k_2} \end{bmatrix} = \begin{bmatrix} 1 \\ \tau \\ \vdots \\ \tau^{N-1} \end{bmatrix}$$

When $|k_2 - k_1| = N - 1$, the coefficient matrix is a Vandermonde matrix and is always invertible. Thus, the filter coefficients have a unique solution. Table II shows some of the 1-D Neville filters of even order, which are all symmetric and thus have linear phase.

TABLE III

QUINCUNX NEVILLE FILTERS

		Numerator							Denominator
Taps	Order\Ring	1(4)	2(8)	3(4)	4(8)	5(8)	6(4)	7(8)	
4	2	1							2^2
12	4	10	-1						2^5
24	6	174	-27	2	3				2^9
44	8	23300	-4470	625	850	-75	9	-80	2^{16}

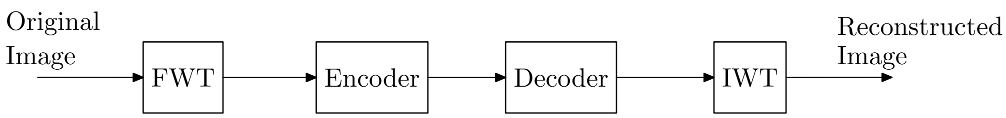

Fig. 7. Block diagram of the compression system

2) Quincunx Filter Banks: In quincunx lattices, the delay between the two sublattices, represented by the filled and unfilled circles in Fig. 5, is $t = \begin{bmatrix} 1 & 0 \end{bmatrix}$, and the shift for the Neville filters is $\tau = D^{-1}t = \begin{bmatrix} 1/2 & 1/2 \end{bmatrix}$. The coefficients of the predict and update filters are selected in the neighborhood of τ in a symmetric way as shown in Fig. 6. The filter coefficients are taken from TABLE II in [4], as shown in table III, where the third to the ninth columns correspond to the tap weights of the seven rings in Fig. 6 numbered from one to seven.

B. Implementation of the Compression System

The compression system is shown in the block disgram in Fig. 7, which includes two parts: two-dimensional wavelet transforms and a coder/decoder.

1) Wavelet Transforms: For the traditional 1-D filter banks, the subband decomposition is applied to the images row-wise first and then column wise. There are four subbands after the first level of decomposition: vertically and horizontally lowpass (LL), horizontally lowpass and vertically highpass (LH), horizontally highpass and vertically lowpass (HL), and vertically and horizontally highpass (HH) subbands. Then the LL band is decomposed further. This two-dimensional forward wavelet transform is in a tree structured 2-D analysis filter bank which results in the subband structure in Fig. 8(a)

For the quincunx filter banks, the input image is decomposed into two subbands after each level of decomposition, and the subbands have the shape of a diamond. The lowpass subband is decomposed

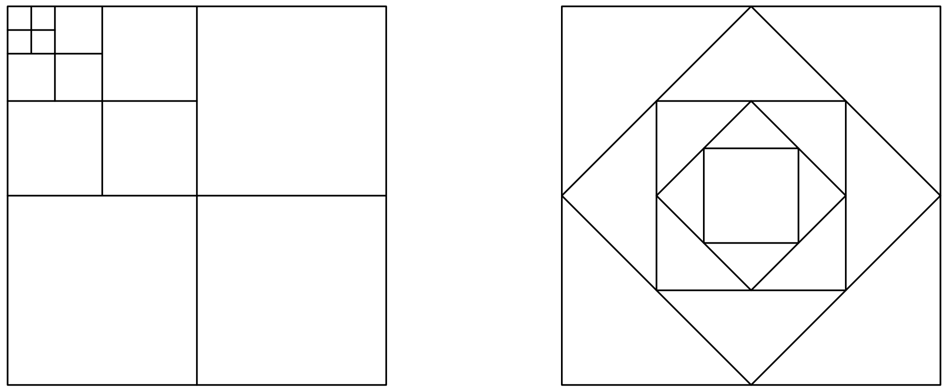

(a) 1-D (b) Quincunx

Fig. 8. The subband structure after four levels of decomposition for the one dimensional filter banks and quincunx filter banks

further. This filter bank results in the subbands structure in Fig. 8(b).

A tree-structure 2-D synthesis filter bank is used to perform the inverse 2-D wavelet transform for the reconstruction of the images. This structure is simply the inverse of the analysis filter bank.

The forward and inverse wavelet transforms are implemented using the lifting steps in Fig. 4. One of the advantages of the lifting structure is that the transform can be calculated in place. Therefore, unlike the subband structure shown in Fig. 8, the wavelet coefficients are stored at their original positions. This leads to the fact that the coefficients belonging to the same subband are not stored next to each other, but scattered in the entire data matrix.

After each lifting step, there is a rounding unit, such that the wavelet coefficients are all signed integers. This unit can be a rounding to zero, to the nearest integer, or flooring after plus $1/2$. As long as the same method is used in the analysis and synthesis sides, the image can still be perfectly reconstructed.

When filtering along the image borders, the filter may need undefined sample points outside the image. There are some schemes for extension, such as symmetric extension and periodic extension. In this project, those undefined sampling points are replaced by their nearest defined neighbor in the same coset. In both one dimensional and quincunx filter banks, the nearest neighbor may not be unique. There may be two points inside the defined region with the same distance an undefined point. However, as long as the selection scheme is the same in the analysis and synthesis side, the image can still be reconstructed.

2) CODEC: The coding algorithm is a simplified version of the EBCOT (embedded block coding with optimized truncation) [5] used in JPEG 2000. Compared to other popular coding schemes, such as EZW [6] and SPIHT [7], EBCOT does not employ the interband information, thus it can be used in both separable and nonseparable subband decompositions. I tried to write one that can address both the lossy and lossless coding, but the time is not enough, therefor only the lossless part in included.

The encoder works in a similar way to that in JPEG 2000 [8] [5] [9] [10] as follows. Each subband is processed separately. The wavelet coefficients of a subband are arithmetically coded by bitplane. The coding is performed from the most significant bitplane to the least significant bitplane. For 1-D filter banks, each bitplane is scanned in the order in Fig. 9. In quincunx case, when there are odd levels of decomposition, the subbands have the shape of a diamond. The scan order is the same except for a rotation of $45°$, as I stored the subband signals in a rectangular matrix.

Encoding a bit involves (1) determining its context, (2) estimating a probability for it, and (3) sending the bit and its probability to an arithmetic coder, named MQ coder. Each wavelet coefficient has a 1-bit variable indicating its significance. The context of a bit is computed from the significance of its eight near neighbors.

There are three coding passes per bitplane. Each bit in the bitplane is encoded in one of the three passes. The first coding pass, the significance propagation pass, encodes all the bits that belong to the wavelet coefficients satisfying:

- the coefficient is insignificant
- at least one of its eight nearest neighbors is significant

If a bit encoded in this pass is 1, its wavelet coefficient is marked as significant. The second coding pass, the magnitude refinement, encodes all bits of wavelet coefficients that became significant in a previous bitplane. The third coding pass, the cleanup pass, encodes all the remaining bits in the bitplane. If a bit encoded in this pass is 1, the wavelet coefficient becomes significant.

Encoding starts from the first bitplane that is not identically zero, and this bitplane is encoded in the cleanup pass. The sign bit of a coefficient is encoded following the first 1 bit of the coefficient.

The context of a bit is determined in different ways for different passes. For one-dimensional transforms, the decision is the same as in JPEG2000 [8]. For quincunx transforms, the lowpass band uses the contexts for the LL subband, and the highpass band uses the contexts for the HH subband.

The code in this part relies on the JasPer software [11].

3) Quantization: Since the CODEC does not work, a simple quantization is used to simulate a lossy coder. One of the quantization strategy is to throw away several least significant bitplanes of the wavelet coefficients. This can be done by shifting the bits of every coefficient.

Another quantization strategy that works well for 2-D subband signals is to apply a hard thresholding with threshold δ to the images [12], which results in more zero coefficients and thus increases the

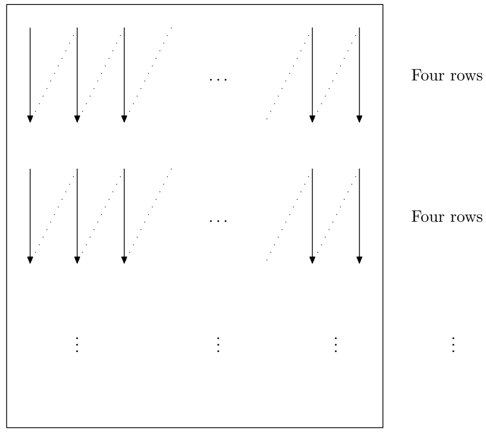

Fig. 9. Scan order within a subband

”compression ratio” η defined as

$$\eta = \frac{k_0}{k} \tag{2}$$

where k_0 is the number of pixel in the original image with magnitude larger than δ, and k is the number of wavelet coefficients after the forward wavelet transform with magnitude larger than δ. All the coefficients that are less than or equal to δ are set to zero.

C. Performance Comparison

The criterion for performance comparison is the bit rate (bit per pixel) in the compressed data.

For lossy coding, the PSNR (peak signal to noise ratio) and visual quality is used, where the PSNR and MSE (mean squared error) is defined as:

$$\text{PSNR} = 10 \log_{10} \frac{\left(2^P - 1\right)^2}{\text{MSE}}$$

$$\text{MSE} = \frac{1}{MN} \sum_{i=0}^{M-1} \sum_{j=0}^{N-1} \left(x_{i,j} - \hat{x}_{i,j}\right)^2$$

If the hard thresholding strategy is used to quantize the wavelet coefficients, η as defined in (2) can also serve as a criterion.

V. Results

A. Examples of Interpolating Filter Banks

1) Haar: Haar filter bank is the simplest filter bank with $N = 1$ primal and $\tilde{N} = 1$ dual vanishing moments. The predict and update filters are $P(z) = 1$ and $U(z) = 1/2$ respectively. The corresponding

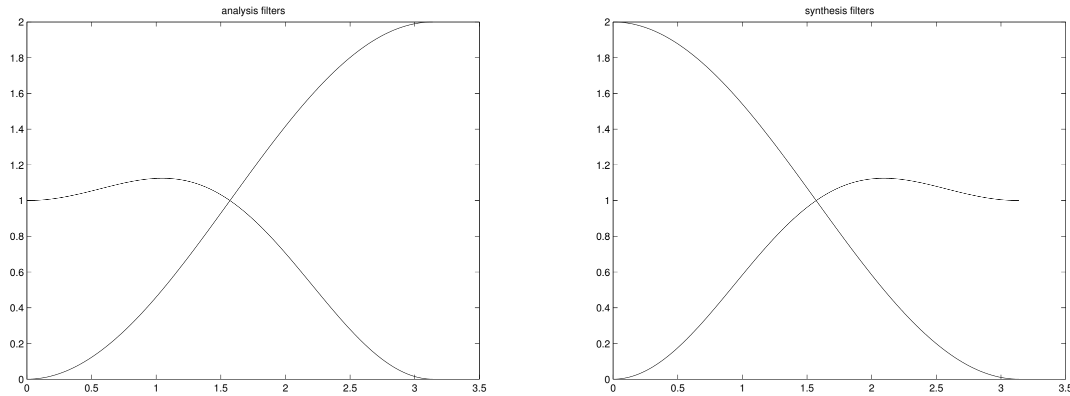

(a) Analysis filters (b) Synthesis filters

Fig. 10. Frequency responses of the analysis and synthesis filters with $N = 2$ primal and $\tilde{N} = 4$ dual vanishing moments

filters are $H(z) = 1 + z^{-1}$ and $G(z) = -1/2 + z^{-1}/2$.

2) One Dimensional Filter Bank with $N = 2$ primal and $\tilde{N} = 4$ dual vanishing moments: The predict filter is a Neville filter of order 4, and two times the adjoint of the update filter is a Neville filter of order 2, therefore

$$P(z) = \left(-z + 9 + 9z^{-1} - z^{-2}\right)/16$$
$$U(z) = (z + 1)/4$$

And the corresponding analysis lowpass and highpass filters are:

$$\tilde{H}(z) = \left(z^4 - 8z^2 + 16z + 46 + 16z^{-1} - 8z^{-2} + z^{-4}\right)/64$$
$$\tilde{G}(z) = \left(z^2 - 9 + 16z^{-1} - 9z^{-2} + z^{-4}\right)/16$$

The frequency responses of the analysis and synthesis filters are shown in Fig. 10

3) Quincunx Filter Bank with $N = 2$ primal and $\tilde{N} = 2$ dual vanishing moments: The predict filter is a two dimensional Neville filter of order 2, and two times the adjoint of the update filter is also a Neville filter of order 2, therefore

$$P(z) = \left(1 + z_1^{-1} + z_2^{-1} + z_1^{-1}z_2^{-1}\right)/4$$
$$U(z) = (1 + z_1 + z_2 + z_1 z_2)/8$$

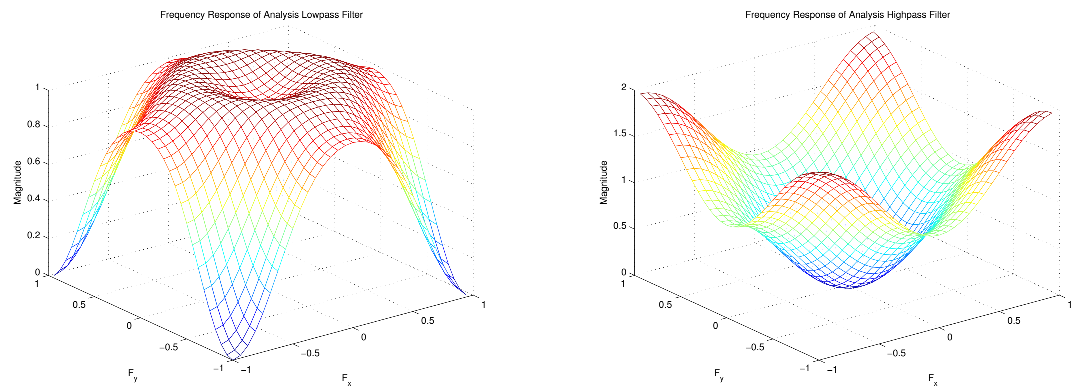

(a) Analysis filters (b) Lowpass filter

Fig. 11. Frequency responses of the quincunx lowpass and highpass filters with $N = 2$ primal and $\tilde{N} = 2$ dual vanishing moments

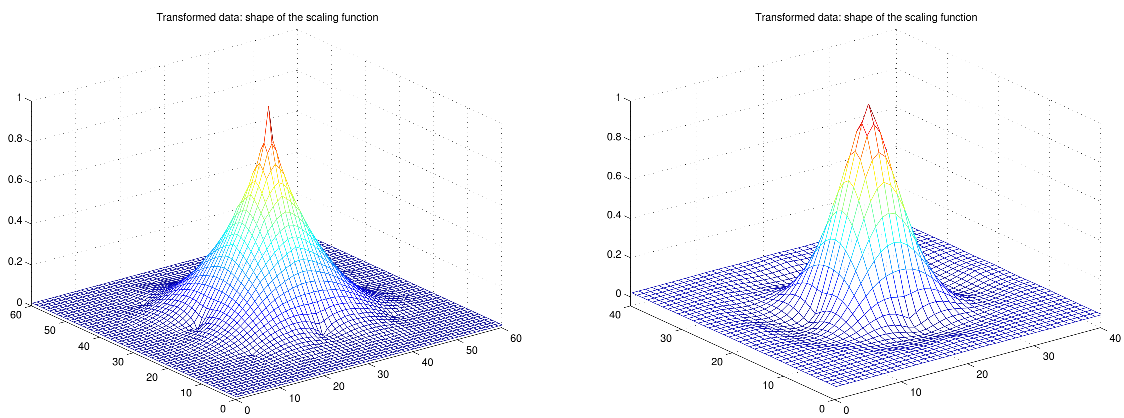

(a) Quincunx 2/2 (b) Quincunx 4/4

Fig. 12. The approximation of the scaling functions of two members of the quincunx filter banks family

And the corresponding analysis lowpass and highpass filters are:

$$\tilde{H}(z) = \frac{1}{32}\left(28 - 2z_1^{-1}z_2^{-1} - 2z_1z_2^{-1} - 2z_1^{-1}z_2 - 2z_1z_2 - z_1^{-2} - z_1^2 - z_2^{-2} - z_2^2 + 4z_1^{-1} + 4z_1 + 4z_2^{-1} + 4z_2\right)$$

$$\tilde{G}(z) = z_1^{-1} - \left(1 + z_1^{-1}z_2^{-1} + z_1^{-1}z_2 + z_1^{-2}\right)$$

This results in the frequency responses of the lowpass and highpass filters shown in Fig. 11. This combination does not leads to a stable biorthogonal basis. An approximation of the shape of the scaling function is shown in Fig. 12(a), and the shape of the scaling function of another quincunx filter bank is shown in Fig. 12(b).

TABLE IV

FILE SIZE OF 3 AND 4 LEVELS OF DECOMPOSITION

		Number of Primal/Dual Vanishing Moments							
Image	Levels	1/1	1/2	2/2	2/4	4/4	2/6	4/6	2/2
lena	3	1213	1310	1043	913	1047	883	882	4240
	4	973	1093	793	644	768	622	615	4349
man	3	1703	1692	1299	1136	1023	1098	1098	7238
	4	1485	1455	1034	854	1309	812	812	7543

TABLE V

FILE SIZE OF 4 AND 5 LEVELS OF DECOMPOSITION

		Number of Primal/Dual Vanishing Moments							
Image	Levels	2/2	2/4	4/4	2/6	4/6	2/8	4/8	6/8
airplane	4	2170	1933	1858	1878	1849	1863	1849	1874
	5	1601	1351	1305	1299	1297	1272	1302	1279

B. Performance Comparison

The nine test images are all 8-bit gray images, with the size of 512×512.

1) Lossless: The lossless encoder creates a file containing the compressed data. The bit rate is given by the size of the compressed data over the number of pixels in the original image. The encoder does not work correctly, as the size is unreasonably small, and so far I still has not figured out where the problem is. Although the encoder is wrong, the size of the output file seems to be proportional to what it should be. For example, more decomposition levels and long filters results in smaller size. I think perhaps the encoder codes only a small part of the subband data, and the results may represent some of the properties of the filter banks.

Table IV shows the compression results from 1-D interpolating filter banks with different numbers of vanishing moments. Table V are the results from quincunx filter banks. It can be seen from Table IV that the two nonsymmetric filters perform the worst for all the images. Especially the one list in the last column with causal predict filter. Its output file size is much larger than the others. Another nonsymmetric filter is in the fourth column with one primal and two dual vanishing moments. It can be seen from the table that longer filters generally perform better than shorter ones, and more levels of decomposition leads to higher compression ratio.

2) Lossy: The performance from simple quantization strategies that simulate the lossy coding is shown in this part. Firstly, several least significant bitplanes of all the wavelet coefficients are simply thrown away, and the image is reconstructed using the wavelet coefficients with less precision. The PSNR and number of zero coefficients are computed and the results are shown in Tables VI - IX.

Using this strategy, small coefficients are lost and large coefficients are quantized to an integer power of 2. Table VI shows the results from various 1-D filter banks of 4 levels of decomposition on different images. In the quantization step, three least significant bitplanes are thrown away. It shows that the filter bank in the rightmost column performs the worse, which is the non symmetric filter banks. The filter bank with 1 primal and 2 dual vanishing moments seem to have the best reconstruction, as the PSNR is the highest for all the test images, but the number of zero coefficients are much less than the symmetric filters with more vanishing moments, which may lead to a low compression ratio. The analysis lowpass filter of this filter bank is not symmetric: $\tilde{H}(z) = 0.75 + 0.5z^{-1} - z^{-2}$.

The filter bank with 2 primal and 2 dual vanishing moments gives the second best PSNR for all, and it has a number of zero coefficients comparable to the longer filters. The analysis lowpass and highpass filters of this filter bank is

$$\tilde{H}(z) = \frac{1}{8}\left(-z^2 + 2z + 6 + 2z^{-1} - z^{-2}\right)$$
$$\tilde{G}(z) = \frac{1}{2}\left(-1 + 2z^{-1} - z^{-2}\right)$$

which is the unnormalized CDF22 filter bank.

Table VII gives the results of quincunx filter banks with 8 levels of decomposition, thus the lowpass subband has the same number of samples as the 1-D filter banks in Table VI. Again, the three least significant bitplanes are thrown away. These quincunx filters have symmetric filters. For all the test images, the filter bank with the least vanishing moments (2/2) gives the best PSNR. The numbers of different filter banks do not vary too much, although longer filters tend to have more zero coefficients. Combine Table VI and VII, the quincunx filter banks generally have higher PSNR but less zero coefficients.

Table VIII shows the results from the one-dimensional filter banks with 6 levels of decomposition. Different numbers of bitplanes are shifted out. It can be seen from the table that with higher levels of decomposition, the nonsymmetric (1/2) filter bank is no longer the best in terms of PSNR, while the one with 2 primal and 2 dual vanishing moments still performs very well.

Table IX shows the results from the quincunx filter banks with 12 levels of decomposition. Different numbers of bitplanes are shifted out. The one with two primal and two dual vanishing moments still performs the best in terms of PSNR.

TABLE VI

PERFORMANCE OF 1-D FILTER BANKS ON DIFFERENT IMAGES, WITH THREE BITPLANES THROWN AWAY

		Number of Primal/Dual Vanishing Moments							
Image	Criterion	1/1	1/2	2/2	2/4	4/4	2/6	4/6	2/2
airplane	# of zeros	220138	231199	232875	**234967**	234719	234868	234782	204689
	PSNR	32.77	**33.68**	**33.64**	33.24	32.77	33.03	32.47	28.35
baboon	# of zeros	125183	133321	140150	141081	**142076**	140532	141683	89956
	PSNR	31.83	**33.17**	**32.75**	32.25	31.69	32.02	31.45	27.155
barb	# of zeros	169989	187274	193233	198738	200373	200017	**201827**	152256
	PSNR	32.31	**33.40**	**33.02**	32.32	32.21	32.24	31.95	27.61
boat	# of zeros	179030	191736	197130	197698	**197869**	197000	197400	143889
	PSNR	32.44	**33.45**	**33.02**	32.45	32.29	32.30	32.04	27.38
fruits	# of zeros	226380	232075	235205	235843	**235856**	235617	235770	196734
	PSNR	32.96	**34.10**	33.71	**33.34**	33.05	33.02	32.73	27.76
goldhill	# of zeros	183179	197452	202282	202052	**202311**	200989	201285	149295
	PSNR	32.33	**33.32**	**32.99**	32.45	32.04	32.29	31.88	27.41
lena	# of zeros	208867	224934	228412	230269	**230305**	229942	230223	182646
	PSNR	32.69	**33.74**	**33.42**	32.79	32.76	32.54	32.52	27.65
man	# of zeros	189844	202873	207406	**208820**	208760	208076	208208	162018
	PSNR	32.40	**33.66**	**33.03**	32.52	32.20	32.23	31.95	27.57
peppers	# of zeros	209740	220132	**224347**	223494	223723	222358	222859	174373
	PSNR	32.63	**33.70**	**33.45**	32.98	32.70	32.69	32.44	27.53

Another quantization strategy is the hard thresholding as stated in the previous section. After the quantization, the small coefficients are set to zero, while the large coefficients remains the same, unlike in the bitplane method where they are quantized to an integer power of 2. The performance results are shown in Tables X - XIII.

Table X shows the results from various 1-D filter banks of 4 levels of decomposition on different images. The threshold is set to 15. The nonsymmetric filters, which are in the fourth and rightmost columns, and the Haar filter banks are the worst, as the ratio η and the PSNR are both low. Among the other filter banks, the 2/2 one has the best PSNR, but ”compression ratio” is lower. It seems the other four, with 2/4, 4/4, 2/6, and 4/6 vanishing moments respectively, have η and PSNR that are close to each other.

Table XI is the counterpart to Table X, with quincunx filter banks of 12 levels decomposition, and

TABLE VII

PERFORMANCE OF QUINCUNX FILTER BANKS ON DIFFERENT IMAGES. THREE BITPLANES ARE THROWN AWAY

		Number of Primal/Dual Vanishing Moments							
Image	Criterion	2/2	2/4	4/4	2/6	4/6	2/8	4/8	6/8
airplane	# of zeros	223739	230242	231018	231006	**231272**	231197	231247	230959
	PSNR	**33.81**	33.29	32.34	33.02	32.13	32.87	31.97	32.72
baboon	# of zeros	127737	131298	130789	131548	130216	130980	129367	**131706**
	PSNR	**33.59**	32.78	31.26	32.42	30.99	32.28	30.91	31.82
barb	# of zeros	176228	183766	183331	186238	185137	187559	186187	**189039**
	PSNR	**33.45**	32.72	31.40	32.51	31.21	32.44	31.15	31.91
boat	# of zeros	188043	192168	191705	**191883**	190610	191100	189338	191683
	PSNR	**33.50**	32.72	31.27	32.52	31.09	32.40	30.95	32.10
fruits	# of zeros	228960	231172	**231588**	231246	231086	230925	230529	230869
	PSNR	**34.17**	33.45	32.33	33.11	32.10	32.90	31.98	32.70
goldhill	# of zeros	190084	195665	195902	196309	195668	196197	195091	**196493**
	PSNR	**33.52**	32.87	31.50	32.53	31.26	32.50	31.20	31.90
lena	# of zeros	221820	226838	227012	227309	227038	227208	226601	**227318**
	PSNR	**33.71**	33.02	31.93	32.76	31.64	32.60	31.56	32.50
man	# of zeros	197254	202157	**202912**	202189	202225	201857	201323	201637
	PSNR	**33.65**	32.89	31.51	32.62	31.52	32.50	31.36	31.99
peppers	# of zeros	224134	224860	**224399**	223964	222759	223130	221534	223658
	PSNR	**33.75**	32.96	31.91	32.89	31.81	32.56	31.65	32.48

the threshold $\delta = 15$. The filter bank with two primal and two dual vanishing moments has the highest PSNR for all the images, as in the bitplane method, but the compression ratio is lower, especially for some of the images. The best one in terms of the ratio η varies among the filter banks with at least 6 dual vanishing moments. Combine with Table X the quincunx filters generally offers lower compression ratio and higher PSNR.

Table XII and Table XIII show the results of various threshold on Lena with 6-level 1-D filter banks and 12-level quincunx filter banks, respectively. Among 1-D filter banks, the (2/2) filter bank still performs well on PSNR except in the last case with high compression ratio. The other four, in the first to fourth columns from the right, has similar performance. Similarly, in the quincunx case, the (2/2) filter bank has the highest PSNR and lowest compression ratio.

The images processed with different wavelet transforms are also compared in terms of visual quality.

TABLE VIII

PERFORMANCE OF 1-D FILTER BANKS WITH DIFFERENT NUMBERS OF BITPLANES

		Number of Primal/Dual Vanishing Moments						
# of Bitplanes	Criterion	1/1	1/2	2/2	2/4	4/4	2/6	4/6
1	# of zeros	77923	86611	91415	91205	**91471**	90231	90667
	PSNR	39.31	39.90	**42.06**	41.07	40.35	40.79	40.55
2	# of zeros	148540	165177	171335	172003	**172387**	170948	171743
	PSNR	35.38	36.67	**37.78**	36.63	36.54	36.09	36.15
3	# of zeros	209287	225224	228781	230658	**230690**	230328	230613
	PSNR	31.11	32.36	**32.60**	31.39	31.27	31.23	30.67
4	# of zeros	241458	248599	250063	251421	251435	251561	**251677**
	PSNR	25.63	27.22	**27.34**	26.26	26.01	26.10	25.63
5	# of zeros	256034	257508	258318	258875	258811	258993	**258994**
	PSNR	20.24	21.51	**21.76**	21.19	20.94	21.00	20.62
6	# of zeros	261251	261045	261404	261601	261574	261619	**261621**
	PSNR	15.31	**15.73**	15.64	15.07	14.90	14.79	14.71

TABLE IX

PERFORMANCE OF QUINCUNX FILTER BANKS WITH DIFFERENT NUMBERS OF BITPLANES

		Number of Primal/Dual Vanishing Moments							
# of Bitplanes	Criterion	2/2	2/4	4/4	2/6	4/6	2/8	4/8	6/8
1	# of zeros	88830	**90407**	90069	89241	88518	88287	87134	89136
	PSNR	43.75	42.57	**44.02**	42.42	43.44	41.57	42.81	41.22
2	# of zeros	166466	**170073**	169448	169145	167959	168123	166581	169119
	PSNR	**37.04**	36.42	36.93	36.15	36.31	35.93	35.84	36.34
3	# of zeros	222080	227091	227280	227564	227291	227474	226859	**227584**
	PSNR	**32.57**	31.63	30.94	31.58	30.65	31.08	29.93	31.10
4	# of zeros	246353	249563	250016	250132	250259	**250293**	250187	250221
	PSNR	**27.32**	26.18	24.89	25.71	24.77	25.95	24.23	25.34
5	# of zeros	257322	258636	258865	258917	258930	**258993**	258901	258974
	PSNR	**21.82**	20.67	20.00	20.40	19.77	20.32	19.66	20.11
6	# of zeros	261312	261607	261667	261675	261647	261697	261631	**261722**
	PSNR	**15.81**	15.07	14.62	14.69	14.36	14.61	14.26	14.44

TABLE X

PERFORMANCE OF 1-D FILTER BANKS ON DIFFERENT IMAGES WITH THRESHOLD 15

		Number of Primal/Dual Vanishing Moments							
Image	Criterion	1/1	1/2	2/2	2/4	4/4	2/6	4/6	2/2
airplane	η	12.83	18.34	20.00	22.49	22.21	**23.12**	23.03	9.14
	PSNR	31.79	32.59	**33.19**	32.40	32.48	32.03	32.16	25.44
baboon	η	3.45	3.76	4.14	4.23	**4.26**	4.21	**4.26**	2.26
	PSNR	28.53	29.62	**30.10**	29.31	29.47	29.06	29.17	24.82
barb	η	4.98	6.13	6.99	7.77	8.02	8.04	**8.32**	3.85
	PSNR	29.93	30.74	**31.37**	30.70	30.95	30.49	30.66	24.83
boat	η	7.86	10.77	12.00	**12.39**	12.34	12.18	12.20	4.64
	PSNR	29.75	30.43	**30.99**	30.33	30.51	30.14	30.27	23.94
fruits	η	18.48	22.10	25.09	27.22	27.02	27.52	**27.62**	8.15
	PSNR	31.32	32.40	**33.04**	32.31	32.42	32.05	32.14	24.52
goldhill	η	9.19	11.80	13.37	13.83	13.88	13.81	**13.93**	4.76
	PSNR	29.26	30.07	**30.69**	30.07	30.19	29.79	29.89	23.96
lena	η	12.31	18.72	20.81	23.24	23.26	23.53	**23.76**	7.45
	PSNR	30.82	31.88	**32.56**	31.95	32.10	31.68	31.83	24.31
man	η	8.36	10.26	11.51	12.20	12.17	12.21	**12.25**	4.67
	PSNR	29.67	30.52	**31.15**	30.42	30.51	30.08	30.23	24.65
peppers	η	15.10	23.26	24.48	**26.32**	26.13	26.00	25.99	7.89
	PSNR	30.73	31.88	**32.65**	31.79	31.96	31.50	31.56	23.80

- *Example 1:* Fig. 13(a) is the reconstructed image from three levels of decomposition of the MIT9/7 filter banks, which has two primal and four vanishing moments. Fig. 13(b) is the reconstructed image from Haar filter bank, which has one primal and one dual vanishing moments. The three least significant bitplanes are thrown away. It can be seen that although the PSNR is almost the same, the quality of Fig. 13(a) is much better than Fig. 13(b), as Fig. 13(b) has the severe blocking effects.
- *Example 2:* Fig. 14 shows the reconstructed images with low PSNR. Fig. 14(a) is the reconstructed image from six levels of decomposition of the quincunx filter banks with two primal and two vanishing moments. Fig. 14(b) is the reconstructed image from three levels of decomposition of the MIT9/7 filter banks, which has two primal and four vanishing moments. These two subband decompositions result in the same number of the wavelet coefficients in the lowpass subbands. The PSNR of the quincunx filter bank is only a little higher, but the quality is better the MIT97 filter

(a) MIT9/7, 2 primal and 4 dual vanishing moments

(b) Haar: 1 primal and 1 dual vanishing moments

Fig. 13. Reconstructed image by throwing away three least significant bitplanes with 1-D filter banks

(a) Quincunx filter bank with 2 primal and 2 dual vanishing moments

(b) MIT97 filter bank

Fig. 14. Reconstructed image by throwing away five least significant bitplanes

TABLE XI

PERFORMANCE OF QUINCUNX FILTER BANKS WITH THRESHOLD 15

		Number of Primal/Dual Vanishing Moments							
Image	Criterion	2/2	2/4	4/4	2/6	4/6	2/8	4/8	6/8
airplane	η	14.55	18.44	19.08	19.93	20.21	21.02	**21.11**	20.61
	PSNR	**33.68**	32.56	31.18	32.00	30.92	31.78	30.70	32.19
baboon	η	3.45	3.64	3.61	3.67	3.60	3.67	3.58	**3.71**
	PSNR	**30.87**	29.86	28.77	29.43	28.47	29.18	28.27	29.43
barb	η	5.16	5.78	5.68	6.03	5.88	6.15	5.96	**6.37**
	PSNR	**31.92**	30.64	29.62	30.30	29.26	30.08	29.17	30.31
boat	η	9.03	10.53	10.72	10.74	**10.84**	10.64	10.64	10.79
	PSNR	**31.50**	30.41	29.15	28.88	29.84	28.72	28.72	30.14
fruits	η	19.09	22.65	23.29	23.31	23.34	**23.47**	23.12	23.28
	PSNR	**33.25**	32.22	30.95	31.83	30.59	31.49	30.36	31.78
goldhill	η	10.33	11.93	12.03	12.26	12.02	12.33	11.88	**12.43**
	PSNR	**31.06**	30.14	29.01	24.75	28.72	29.52	28.55	29.86
lena	η	16.22	20.13	20.83	21.01	21.23	**21.26**	21.12	21.12
	PSNR	**32.67**	31.70	30.30	31.27	30.07	31.09	30.04	31.45
man	η	9.37	10.77	10.94	**11.01**	10.92	11.00	10.77	**11.01**
	PSNR	**31.67**	30.52	29.20	30.08	28.91	29.87	28.79	30.07
peppers	η	19.49	23.58	23.87	24.89	24.40	**25.53**	24.63	25.42
	PSNR	**32.83**	31.75	30.36	31.26	30.01	30.91	29.82	31.28

bank.

VI. CONCLUSIONS

In this project, several one dimensional and quincunx interpolating filter banks are built using the method proposed by Kovačević and Sweldens in [4]. The construction relies on the lifting structure with two lifting steps. Three important properties: perfect reconstruction, dual and primal vanishing moments, are satisfies separately. Then these filter banks are used to decompose images in a simple image compression system, and their performance are compared.

From the compression results, it can be seen that different filter banks have different effects on the images. Their performance depends on the particular images, levels of decomposition and the desired compression ratio. It is hard to find one that offers the best overall performance. Generally speaking,

TABLE XII

PERFORMANCE OF 1-D FILTER BANKS WITH VARIOUS HARD THREDHOLDING

		Number of Primal/Dual Vanishing Moments						
Threshold	Criterion	1/1	1/2	2/2	2/4	4/4	2/6	4/6
5	η	3.51	4.64	5.09	5.24	**5.27**	5.16	5.21
	PSNR	36.68	37.60	**37.68**	36.75	36.54	36.76	36.65
10	η	7.49	11.31	12.62	13.78	13.78	13.79	**13.91**
	PSNR	31.56	32.87	**33.38**	32.27	32.46	31.95	32.17
20	η	19.30	28.91	33.21	37.81	37.60	37.60	**38.96**
	PSNR	26.27	28.03	**28.81**	27.73	27.61	27.61	27.35
30	η	39.90	53.65	64.49	75.29	74.14	**78.21**	78.19
	PSNR	23.47	24.71	**25.84**	24.72	24.89	24.40	24.41
60	η	214.59	178.25	266.62	349.18	333.38	367.77	**373.36**
	PSNR	18.78	**19.82**	19.58	18.72	18.86	18.08	18.30

symmetric filters perform better than nonsymmetric filters, and longer filters with more vanishing moments perform better for smooth images. The filter banks in the quincunx family tend to have higher PSNR but lower compression ratio than those with the same number of vanishing moments in the one-dimensional family.

There are still a lot of unfinished work in this project. Firstly, the encoder needs to be corrected, such that the performance can be compared in a more reasonable way, and the compression results need to be examined more carefully. More future work includes studying the performance of other families of one dimensional wavelet transforms and wavelet transforms on other nonseparable sampling lattices.

REFERENCES

[1] G. Strang and T. Nguyen, *Wavelets and Filter Banks*. Wellesley, MA: Wellesley-Cambridge, 1996.

[2] W. Sweldens, “The lifting scheme: A custom-design construction of biorthogonal wavelets,” *Appl. Comput. Harmon. Anal.*, vol. 3, pp. 186–200, 1996.

[3] I. Daubechies and W. Sweldens, “Factoring wavelet transforms into lifting steps,” *J. Fourier Anal. Applicat.*, vol. 4, no. 3, pp. 247–269, 1998.

[4] J. Kovačević and W. Sweldens, “Wavelet families of increasing order in arbitrary dimensions,” *IEEE Trans. Image Processing*, vol. 9, pp. 480–496, Mar. 2000.

[5] D. Taubman, “High performance scalable image compression with ebcot,” *IEEE Trans. Image Processing*, vol. 9, pp. 1158–1170, July 2000.

[6] H. M. Shapiro, “Embedded image coding using zerotrees of wavelet coefficients,” *IEEE Trans. Signal Processing*, vol. 41.

TABLE XIII

PERFORMANCE OF QUINCUNX FILTER WITH VARIOUS HARD THRESHOLDING

		Number of Primal/Dual Vanishing Moments							
Threshold	Criterion	2/2	2/4	4/4	2/6	4/6	2/8	4/8	6/8
5	η	4.51	**4.92**	4.90	**4.92**	4.86	4.87	4.78	**4.92**
	PSNR	**38.76**	37.78	37.26	37.21	36.81	37.04	36.72	37.44
10	η	9.88	11.83	12.11	12.23	12.31	**12.32**	12.18	12.30
	PSNR	**34.52**	33.06	31.77	32.71	31.36	32.25	31.23	32.50
30	η	50.97	69.92	74.14	75.66	75.83	**77.64**	75.77	77.45
	PSNR	**25.86**	24.33	23.06	23.87	22.88	23.77	22.67	23.92
60	η	231.93	350.84	397.54	396.83	379.13	410.08	373.36	**431.70**
	PSNR	**20.56**	18.54	16.71	18.02	16.49	17.90	16.38	18.19

[7] A. Said and W. A. Pearlman, "A new, fast, and efficient image codec based on set partitioning in hierarchical trees," *IEEE Trans. Circuits Syst. Video Technol.*, vol. 6.

[8] "Iso/iec 15444-1: Information technology–jpeg 2000 image coding system–part 1: Core coding system," 2000.

[9] D. Salomon, *Data Compression: The Complete Reference*, 2nd ed. New York: Springer-Verlag New York, Inc., 2000.

[10] M. D. Adams, "The JPEG-2000 still image compression standard," ISO/IEC JTC 1/SC 29/WG 1 N 2412, Dec. 2002.

[11] ——, "Jasper software reference manual (version 1.700.0)," ISO/IEC JTC 1/SC 29/WG 1 N 2415, Feb. 2003.

[12] W.-S. Lu, *ELEC 459/534 DIGITAL SINGAL PROCESSING III: LECTRUE NOTES*. Department of Electrical and Computer Engineering, University of Victoria, 2003.